

Article

High-Resolution Delay Spread of Wide-Band Wireless Link in Long Tunnels—Theory and Experimental Verification

Yehuda Taragin ^{1,*} , Liat Rapaport ¹ , Niv Elkayam ¹ , Gad A. Pinhasi ²  and Yosef Pinhasi ¹ 

¹ Department of Electrical and Electronics Engineering, Ariel University, Ariel 40700, Israel; liat5300@gmail.com (L.R.); nive@ariel.ac.il (N.E.); yosip@ariel.ac.il (Y.P.)

² Department of Chemical Engineering, Ariel University, Ariel 40700, Israel; gadip@ariel.ac.il

* Correspondence: yehuda.taragin@msmail.ariel.ac.il

Abstract: The need for wireless communication appears everywhere, and with as few interruptions as possible. An extensive and in-depth study has been conducted on the limitations of wireless communication in pedestrian tunnels. Using an analytical mathematical ray tracing model, and performing tunnel measurements, with an autonomous measuring setup, the model was validated. An extraordinary wide band was used for the experiments, which also featured optical systems to ensure accurate results. Since the tunnel is narrow, the differences between the different paths are small, and in order to distinguish them a resolution of 0.2 ns was used. The RMS delay spread, σ_τ , decreases throughout the tunnel, and at no point exceeds 1 ns.

Keywords: experiment; PDP; delay spread; indoor propagation; ray tracing; tunnels; 5G



Citation: Taragin, Y.; Rapaport, L.; Elkayam, N.; Pinhasi, G.; Pinhasi, Y. High-Resolution Delay Spread of Wide-Band Wireless Link in Long Tunnels—Theory and Experimental Verification. *Electronics* **2022**, *11*, 2140. <https://doi.org/10.3390/electronics11142140>

Academic Editors: Lorenzo Rubio and Vicent Miquel Rodrigo Peñarrocha

Received: 22 May 2022

Accepted: 7 July 2022

Published: 8 July 2022

Publisher's Note: MDPI stays neutral with regard to jurisdictional claims in published maps and institutional affiliations.



Copyright: © 2022 by the authors. Licensee MDPI, Basel, Switzerland. This article is an open access article distributed under the terms and conditions of the Creative Commons Attribution (CC BY) license (<https://creativecommons.org/licenses/by/4.0/>).

1. Introduction

Wireless communication has never been more popular [1]. The 5G rates for data and availability are today's standard, with 6G right around the corner [2]. Wireless communication is crucial for performing many of our daily tasks. The reliability of the communication link is a critical issue and in some cases there is no room for error.

One of the primary limitations of wireless communication in tunnels is constructive and destructive interference caused by reflections from walls [3]. However, the influence of each of the components that produce this phenomenon is insufficiently clear. These components may include: the transmission frequency, length and height of the tunnel, the location and polarization of the antennas, the type of tunnel and the roughness of its walls.

One of the main parameters with which the performance of a communication link is measured is root mean square (RMS) delay spread, σ_τ . RMS delay spread describes the duration it takes for all the reflections from a broadcast at a given moment to reach the receiver; in other words, it provides us with the data rate that can be transmitted with the link. Table 1 shows typical RMS delay spread times in different environments.

Table 1. RMS Delay Spread typical values.

| Environment | Center Frequency (MHz) | Bandwidth (MHz) | σ_τ (ns) |
|-------------------------------------|------------------------|-----------------|--------------------|
| Urban—New York City [4] | 910 | 10 | 1300 |
| Suburban [4] | 910 | 10 | 200–310 |
| Indoor—Office Building [5] | 1500 | 500 | 25 |
| Underground Mine Channel [6] | 3500 | 3000 | 11.8 |
| Uneven Underground Mine Channel [7] | 2400 | 200 | 9.92 |

A common approach is to perform an experiment on a specific site without basing the research on any calculations and theoretical model [7–14]. In this form of work, one can learn about a single and specific case, without the ability to generalize to different cases.

Similarly, the opposite case also exists [15,16]: Performing only simulated results, without any experimental verification. This may lead to a situation where a variety of variables are not taken into account while performing the sterile calculations in the simulation, which will lead to invalid results. Therefore, the simulation should be validated with an experiment.

In many studies the bandwidth that was used was very limited [7,12,13,17,18]. This is contrary to the desire to get as high quality results as possible. However, in order to obtain results that accurately reflect the limitations of the tunnel, it is necessary to perform high-resolution measurements. Thus, in order to obtain a higher resolution for measurements in time domain it is necessary to increase the bandwidth in the frequency domain when making the measurements.

Other studies have based their research on experiments with very low measuring resolution [19]: That is, a very limited number of points along the tunnel. Alternatively, the whole length of their experiment was very short [18,20]. In such a situation, it is not possible to get an accurate snapshot, as the signal behavior in the tunnel is not linear or predictable and there are frequent changes along the tunnel.

A common issue in wireless communication experiments is the additional phase added to the results by the measuring equipment. To avoid this phenomenon, fiber optics can be used, since they do not change the phase. Some studies on this subject were aided by fiber optics [19,21], but no in-depth campaign was carried out.

Although similar studies have been previously conducted by other authors, no in-depth and sufficiently accurate investigation has been conducted. In this study, a comprehensive study is conducted on the limitations of wireless communication in tunnels. A frequency range of 1–6 GHz was used to provide an extra large bandwidth of 5 GHz. The large bandwidth in the frequency domain gives us a high resolution in the time domain of 0.2 ns. A long in-depth measurement campaign was carried out in a long pedestrian tunnel. The experimental results were compared to a mathematical model, validating the mathematical model.

2. The Delay Spread Theory in Tunnels and Long Corridors

Electromagnetic wave propagation inside tunnels suffers from multi-path interference, which distorts the received signal due to constructive and destructive waves arriving simultaneously at the receiver. The propagation depends on different parameters such as: Construction materials, antenna polarization, transmitter and receiver location in the cross-sectional area, the separation between the transmitter and receiver, and so on. It is described using (1): [22,23]

$$\tilde{H}_{norm}(jf) = \frac{\tilde{E}_r(Tunnel)}{\tilde{E}_r(LOS)} = \sum_{m=-\infty}^{+\infty} \sum_{n=-\infty}^{+\infty} \underbrace{\frac{R_0}{R(m,n)} \cdot \Gamma_{\alpha}^{|m|} \cdot \Gamma_{\beta}^{|n|} \cdot \frac{G(\theta,\phi)}{G_{LOS}}}_{\tilde{A}_{mn}} \cdot e^{-j2\pi f \Delta\tau(m,n)} \quad (1)$$

$\tilde{H}_{norm}(jf)$ is normalized to the LOS ray for convenience.

$R_0 = R(0,0)$ is the line of sight (LOS) ray length and $R(m,n)$ is the length of the path that the n 'th and m 'th order of reflected ray has traveled, as described in (2):

$$R(m,n) = \sqrt{[x_t(m) - x_r]^2 + [y_t(n) - y_r]^2 + z^2} \quad (2)$$

The image coordinates of the transmitter are defined in (3):

$$x_t(m) = 2ma + (-1)^m \cdot x_t \quad \text{and} \quad x_t(m) = 2ma + (-1)^m \cdot x_t \quad (3)$$

when a represents half of the width of the tunnel and b represents half of the tunnel's height. The reflection coefficient, Γ , is calculated using Fresnel's equations. Since one reflection coefficient will be transverse electric (TE) and the other transverse magnetic (TM) depending on the polarization of the antenna [23,24], they were marked $\Gamma_\alpha^{|m|}$ and $\Gamma_\beta^{|n|}$. m represents the number of reflections in the horizontal dimension, and n is the same but in the vertical dimension. f is the frequency of the wave. For a directive link, $G(\theta, \phi)$ is the geometrical mean gain of both the transmitter and receiver antennas, $G(\theta, \phi) = \sqrt{G_t(\theta, \phi) \cdot G_r(\theta, \phi)}$, and G_{LOS} is the gain of the antenna for the LOS ray.

For simplicity, we define A_{mn} as the following (4):

$$\tilde{A}_{mn} = \frac{R_0}{R(m, n)} \cdot \Gamma_\alpha^{|m|} \cdot \Gamma_\beta^{|n|} \cdot \frac{G(\theta, \phi)}{G_{LOS}} \tag{4}$$

The propagation time for the LOS ray from the transmitter to the receiver is defined in (5):

$$\tau_0 = \frac{R_0}{c} \tag{5}$$

The propagation time delay of each of the other rays is defined as follows (6):

$$\tau(m, n) = \frac{R(m, n)}{c} = \tau_0 + \Delta\tau(m, n) \tag{6}$$

where $\Delta\tau(m, n)$ is the additional time that the (m, n) ray travels more than the LOS ray travels. Assuming the antenna's gain is not dependent on the frequency, the impulse response is:

$$h(t) = \mathcal{F}^{-1}\{\tilde{H}_{norm}(jf)\} = \text{Re}\left\{\int_0^\infty \tilde{H}_{norm}(jf) \cdot e^{+j2\pi ft} df\right\} = \text{Re}\left\{\sum_{m=-\infty}^{+\infty} \sum_{n=-\infty}^{+\infty} \tilde{A}_{mn} \cdot \delta[t - \Delta\tau(m, n)]\right\} \tag{7}$$

The Power Delay Profile (PDP) of the channel, $P_h(\tau)$, describes how much power (from a transmitted delta pulse with unit energy) is transferred to the receiver with a delay of τ from the moment of transmission.

The Power Delay Profile is acquired from the normalized complex impulse response as described in (7) and defined as follows [25]:

$$P_h(\tau) = \frac{|h(\tau)|^2}{\|h(\tau)\|^2} \tag{8}$$

where the norm of $h(\tau)$ is defined by (9):

$$\|h(\tau)\|^2 = \int_{-\infty}^{+\infty} |h(\tau)|^2 d\tau = \int_0^\infty |\tilde{H}_{norm}(jf)|^2 df = \sum_{m=-\infty}^{+\infty} \sum_{n=-\infty}^{+\infty} |\tilde{A}_{mn}|^2 \tag{9}$$

From the last definition, it follows that:

$$\int_{-\infty}^{+\infty} P_h(\tau) d\tau = 1 \tag{10}$$

The PDP is the probability density function (PDF) of the delay τ of an impulse, with dimensions of $[\frac{1}{sec}]$.

The average (mean) delay of all the paths is defined as $\bar{\tau}$ [18]:

$$\bar{\tau} = \langle \tau \rangle = \int_{-\infty}^{+\infty} \tau \cdot P_h(\tau) d\tau = \frac{\sum_{m=-\infty}^{+\infty} \sum_{n=-\infty}^{+\infty} \tau_{mn} \cdot |\tilde{A}_{mn}|^2}{\|h(\tau)\|^2} = \frac{\sum_{m=-\infty}^{+\infty} \sum_{n=-\infty}^{+\infty} \tau_{mn} \cdot |\tilde{A}_{mn}|^2}{\underbrace{\sum_{m=-\infty}^{+\infty} \sum_{n=-\infty}^{+\infty} |\tilde{A}_{mn}|^2}_{\|h(\tau)\|^2}} \tag{11}$$

RMS delay spread, shown as σ_τ in (12), is the standard deviation. In our case, it is an appraisal of the smallest time required between transmission of symbols, in a way that will prevent inter-symbol interference (ISI) [26].

$$\sigma_\tau = \sqrt{\langle \tau^2 \rangle - (\bar{\tau})^2} \tag{12}$$

where

$$\langle \tau^2 \rangle = \int_{-\infty}^{+\infty} \tau^2 \cdot P_h(\tau) d\tau = \frac{\sum_{m=-\infty}^{+\infty} \sum_{n=-\infty}^{+\infty} \tau_{mn}^2 \cdot |\tilde{A}_{mn}|^2}{\underbrace{\sum_{m=-\infty}^{+\infty} \sum_{n=-\infty}^{+\infty} |\tilde{A}_{mn}|^2}_{\|h(\tau)\|^2}} \tag{13}$$

Substituting $\bar{\tau}$ and $\langle \tau^2 \rangle$ into (12), the expression for σ_τ results in (14):

$$\sigma_\tau = \sqrt{\langle \tau^2 \rangle - (\bar{\tau})^2} = \sqrt{\frac{\sum_{m=-\infty}^{+\infty} \sum_{n=-\infty}^{+\infty} \tau_{mn}^2 \cdot |\tilde{A}_{mn}|^2}{\underbrace{\sum_{m=-\infty}^{+\infty} \sum_{n=-\infty}^{+\infty} |\tilde{A}_{mn}|^2}_{\|h(\tau)\|^2}} - \left[\frac{\sum_{m=-\infty}^{+\infty} \sum_{n=-\infty}^{+\infty} \tau_{mn} \cdot |\tilde{A}_{mn}|^2}{\underbrace{\sum_{m=-\infty}^{+\infty} \sum_{n=-\infty}^{+\infty} |\tilde{A}_{mn}|^2}_{\|h(\tau)\|^2}} \right]^2} \tag{14}$$

Since we have described the propagation of the signal in space as rays sent in all directions, it is necessary to specify which rays we will refer to. On the one hand, the number of rays tends to infinity, and on the other hand in terms of mathematical model calculations it is certainly not possible to reach such accuracy.

The number of relevant rays depends very much on the parameters of the communication (wavelength, tunnel size, distance). In an earlier study we conducted [23], we examined the error as a function of the number of rays. We have seen that there is certainly some improvement with the results compared to the experiment as more rays are considered. However, even with a small number of rays the results are satisfactory. To avoid mistakes and inaccuracies, in this study, we took into consideration rays that bounced off the walls up to 30 times and off the ceilings or floor up to 30 times as well, before arriving at the receiver, which is above and beyond any required level of accuracy.

As described, the reflected rays propagate along the tunnel at different times, thus not reaching the receiver simultaneously. In order to paint a clearer picture of this phenomenon, we will demonstrate this by using an example of a tunnel’s impulse response from the model. The model was run in a case that represents the dimensions of the tunnel that will be used in the experiment, as detailed in Table 2. The signal was transmitted at the beginning of the tunnel and recorded at the end of the tunnel.

Table 2. Model example parameters.

| Parameters | Value |
|--------------------------------|----------|
| Frequency | 1.5 GHz |
| Power transmitted | 20 dBm |
| a (half of the tunnels width) | 0.5 m |
| b (half of the tunnels height) | 0.925 m |
| Length | 20 m |
| Material | concrete |

The plot, as shown in Figure 1, visualizes each ray arriving at different times at the receiver. The first ray to arrive represents the LOS ray which has the shortest flight time,

and gradually thereafter all the rest of the rays which did not have a direct path will appear. The Y axis represents normalized values of the received power in relation to the transmitted power.

To present normalized time values of the received arrays in relation to the LOS array, we define (15):

$$t_{normalized} = \frac{L_{m,n} - d}{d} = \frac{\Delta t}{t_r} \quad (15)$$

where $L_{m,n}$ is the distance that the m, n ray travels, d is the length between the transmitter and receiver which the LOS ray travels, in this case $d = 20$ m, Δt is the additional time the m, n ray travels, and t_r is the LOS the ray travels.

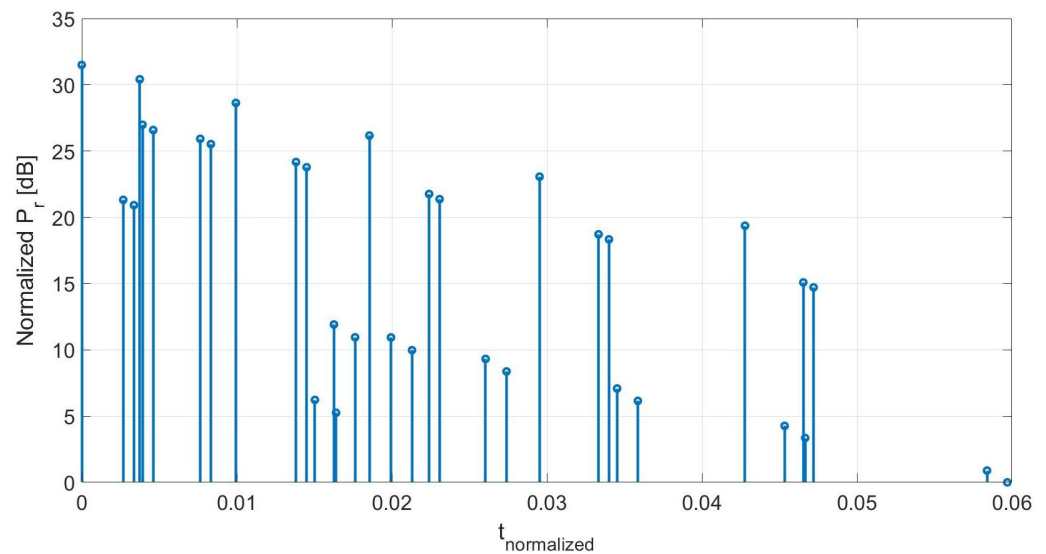


Figure 1. Reflected rays not arriving simultaneously at the receiver.

In the following sections, the analytically calculated and experimental outcome of, inter alia, S_{21} , time domain results and RMS delay spread in a long pedestrian tunnel are presented.

3. Experimental Setup

The measurements were performed in the frequency domain, using a Keysight Streamline USB Vector Network Analyzer (VNA) model number P9371A, as can be seen in Figure 2. A VNA measures the scattering parameters, which describe the relationship between the different ports. A network analyzer is especially useful when the effect of the network in terms of amplitude and phase need to be described. During the experiment, the complex S_{21} parameter was measured, which represents the difference in amplitude and phase between port 1, the transmitter (Tx), and port 2, the receiver (Rx).



Figure 2. Network analyzer.

The VNA is a portable device, allowing for use in the tunnel in order to receive results as accurate as possible. The VNA parameters are detailed in Table 3.

Table 3. Vector network analyzer parameters.

| Parameters | Value |
|-----------------|--------------------|
| Manufacturer | Keysight |
| Model | P9371A |
| Frequency range | 300 kHz to 6.5 GHz |

The transmitting antenna was connected to Port 1, which was placed at the entrance to the tunnel without movement throughout the experiment. In contrast, the receiving antenna, which was connected to Port 2, was moved along the tunnel prior to each measurement.

A broadband horn antenna as shown in Figure 3 was used at both ports, as detailed in Table 4. This was done so that as much power as possible will be in the direction of the transmission, in order to intensify the reflections from the tunnel walls.

**Figure 3.** Wide-band horn antenna.**Table 4.** Wide-band Horn Antenna Parameters.

| Parameters | Value |
|-----------------------|----------------|
| Manufacturer | Chendgu A-INFO |
| Model | JTXLB-10180 |
| Frequency range | 1–18 GHz |
| Gain | 11 dBi Typical |
| Polarization | Linear |
| VSWR | 2.0:1 Typical |
| H-Plane 3dB Beamwidth | 37°–71° |
| E-Plane 3dB Beamwidth | 39.7°–70° |

Although the antenna supports a wide spectrum of frequencies, the antenna gain varies according to the frequency. The gain and antenna factor were measured in an antenna test range, the results of which can be seen in Table 5.

Table 5. Gain and antenna factor.

| Frequency | Antenna Factor (dBm^{-1}) | Gain (dBi) |
|-----------|--------------------------------------|------------|
| 1 | 23.63 | 6.63 |
| 1.5 | 24.18 | 9.6 |
| 2 | 26.03 | 10.25 |
| 3 | 29.8 | 9.98 |
| 4 | 31.60 | 10.7 |
| 6 | 33.97 | 11.85 |

In order to eliminate the uneven frequency response of the antennas, a calibration operation was activated in the VNA prior to the experiment. Thus, the VNA takes into

account the frequency response of the antenna in the calculation of the S_{21} so that the S_{21} only expresses the propagation.

To ensure that the measurement process performs smoothly and gives us the ability to sample the effect of the tunnel many times along the tunnel, an autonomous measuring setup was designed as shown in Figure 4 which parameters are detailed in Table 6.

Table 6. Measurement parameters.

| | |
|-----------------------|---------------|
| Frequency range | 1–6 GHz |
| Number of samples | 11130 |
| Transmission power | 20 dBm |
| Receiver IF bandwidth | 1 kHz |
| Frequency resolution | 0.45 MHz |
| Time resolution | 0.2 ns |
| Maximum excess delay | 2.2 μ sec |

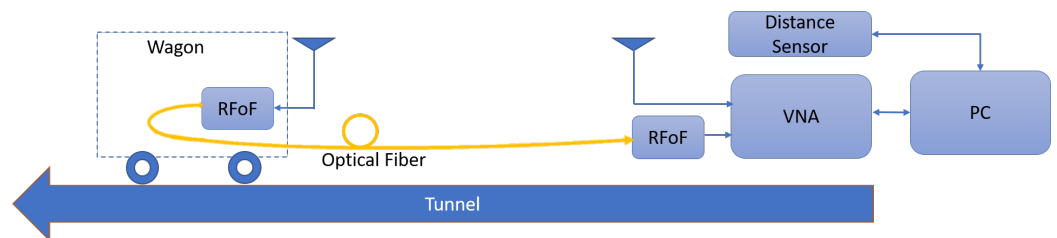


Figure 4. Autonomous measuring setup.

In order to perform autonomous measuring, the VNA was controlled by a PC running Standard Commands for Programmable Instruments (SCPI) coding sent from the MATLAB environment. With the help of this, there was full control over the timing of the measurement and synchronization with the distance data. Additionally, this enabled the results to be stored on the PC for later processing.

In order to accurately measure the distance between the antennas, a Laser Distance Measuring Sensor was used. The distance sensor was connected to the PC via RS232 serial data connection. These serial commands were likewise sent from the MATLAB environment. The laser was placed at the entrance of the tunnel, next to the transmitting antenna. Simultaneously, with each measurement that was performed by the network, a measurement was performed by the distance sensor. In this way, coordinated measurements were obtained.

With the intention of measuring the S_{21} , it is necessary that the receiving antenna will likewise be connected to the network analyzer. Since in the experiment the receiving antenna is on the other side of the tunnel, this phenomenon was accomplished using an optical fiber. The RF signal obtained in the receiving antenna was transformed to an optical signal in order to be transmitted on an optical fiber. The signal traveled through the optical fiber along the tunnel back towards the VNA, which is then converted back to RF before connecting to the VNA. Since the measurements were performed along the tunnel, the separation between the antennas increased with every measurement. With a regular coax cable, every movement causes a change in the phase, and by using an optical fiber this phenomenon is avoided. The additional delay caused by the RF optic device, and the time it took the signal to travel back along the optical fiber, were taken into account and did not affect the measurement results.

The RF Optic device as shown in Figure 5 supports up to 6 GHz with a nominal link gain of 7 dB. The optical signal is transmitted with a 1310 nm wavelength [27]. The device has the ability to increase the signal transmitted via the optical fiber with an LNA. In the experiments, the LNA was not used, since this brought the signal to saturation.



Figure 5. RF-Optic [27].

The experiments were performed in a pedestrian tunnel under a highway. The tunnel is long and straight. The walls are mostly smooth, but there was a certain roughness in between the smooth plates of the concrete. The dimensions of the underpass are: $Height = 2b = 1\text{ m}$, $Width = 2a = 1.85\text{ m}$ and $Length = 75\text{ m}$, as shown in Figure 6a.

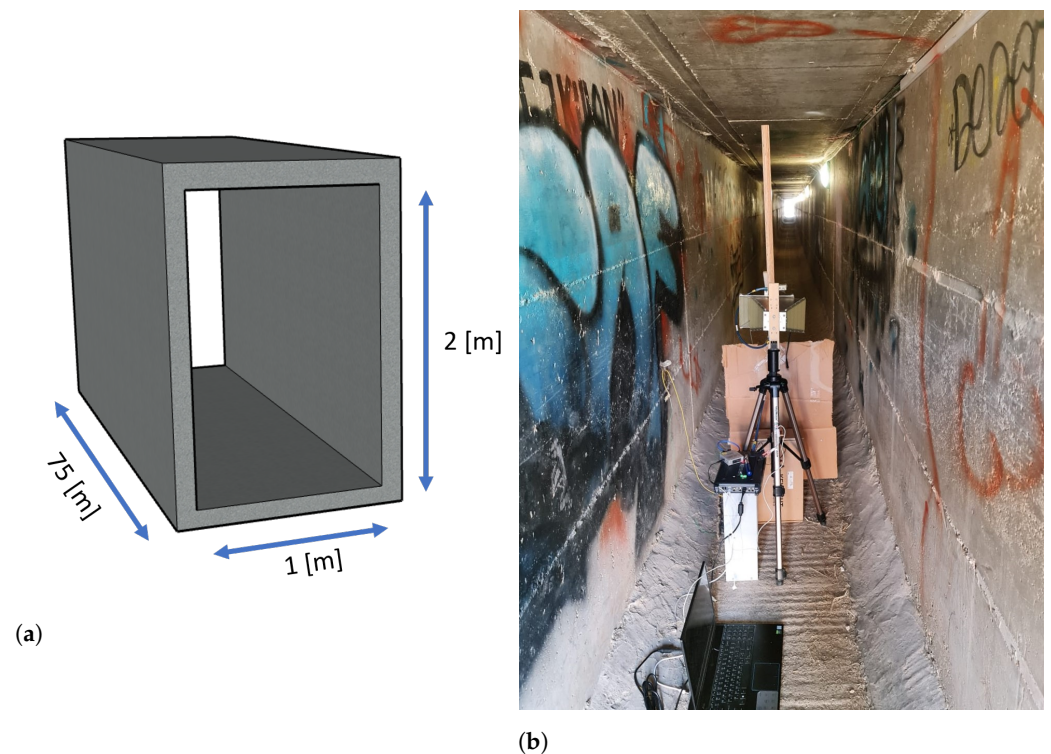


Figure 6. Experiment setup at the experiment site. (a) Illustration of the tunnel dimensions. (b) A photograph taken at the experiment site.

The measurements were carried out along the tunnel, while the transmitting and receiving antennas were placed in the middle of the cross-sectional area of the tunnel. The tunnel was empty throughout the whole measurement process, and therefore there was no interference between the transmitter and receiver.

The transmitter antenna was connected to an antenna stand. The receiving antenna was attached to a pole which was part of the wooden wagon. To give the laser a surface to reflect off of, cardboard was attached to the front of the cart. All components of the experiment were unable to wobble, besides the optical fiber which was loose, enabling it to extend along the tunnel. The experiment setup at the experiment site can be seen in Figure 6b.

4. Tunnel Propagation Characterization via S-Parameters

As a result of the measurements that were performed in the tunnel, the complex S_{21} parameter was obtained along the tunnel. Since the results represent the characteristics of a single tunnel, the results were compared to the simulation results in order to confirm the correctness of the model. In this way, simulation results can be obtained in other unmeasured cases as well, which supplies us with a broader understanding of electromagnetic wave propagation in tunnels.

The first result is essentially one of the basic parameters measured by the network analyzer, the power received versus frequency. The received power was plotted in Figure 7, for 5, 10, 20 and 45 m of distance between the transmitter and receiver. These distances constitute a representative sample along the tunnel. The results from the experiment were plotted with the results from the simulation, so a comparison can be performed between them.

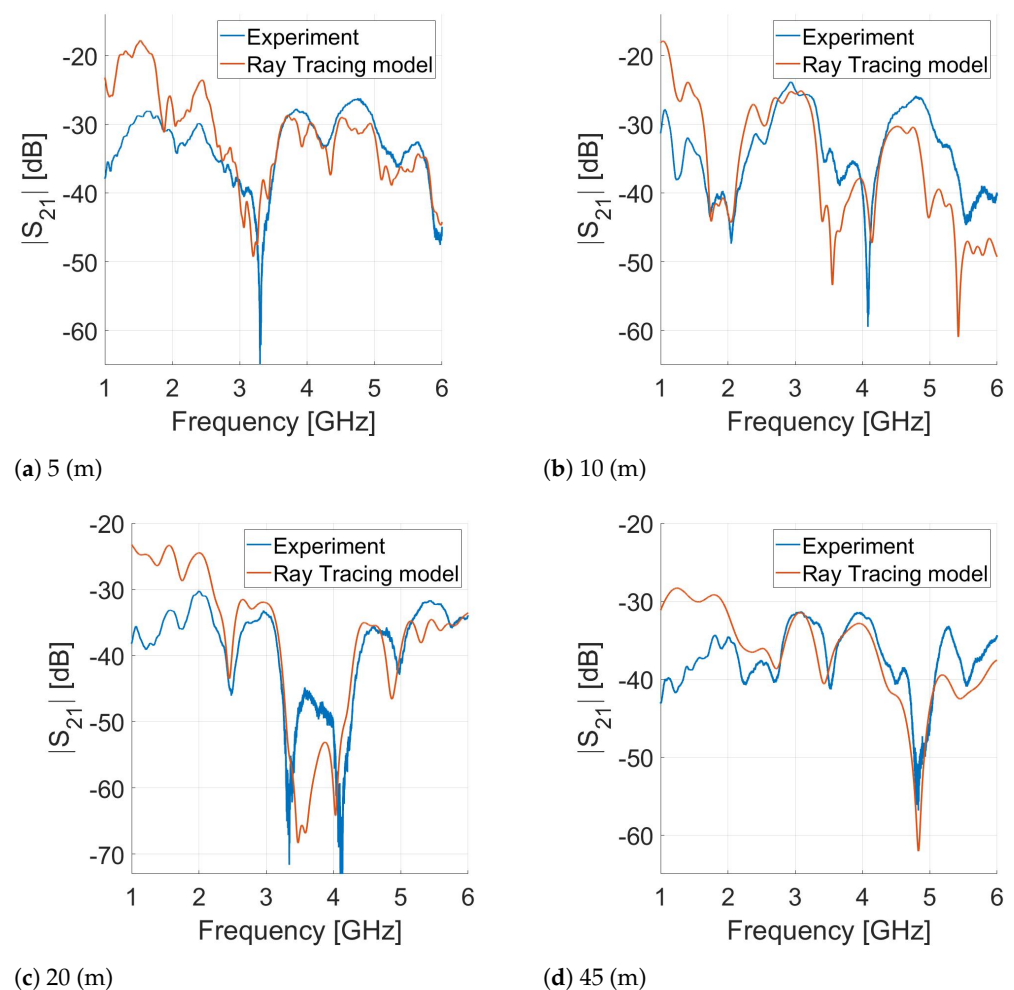


Figure 7. The frequency response of the transmission scattering parameter S_{21} for various distances.

The received power visualizes the selective fading of the frequency that is caused by the tunnel. As is clearly noticeable, the power has peaks and dips in various frequencies, as a consequence of constructive and destructive interference. Hence, the powers received at distinctive frequencies differ from each other.

The experiment results were plotted with the simulation results, so that a comparison can be made between them. The comparison shows a high similarity between the experiment and simulation. Among the general results obtained, there is a good match, but especially in the location of the peaks and dips there is a precise match. The precise match

in the location of the peaks and dips is of high importance since they have the greatest effect on the communication performance, more than the power obtained at any specific location.

5. Power Delay Profile Measurements

The IFFT function was applied to the frequency domain results in the time domain. By doing so we obtained the Power Delay Profile (PDP) as described in (8). The PDP was normalized and plotted in Figure 8, for 5, 10, 20 and 45 m of distance between the transmitter and receiver.

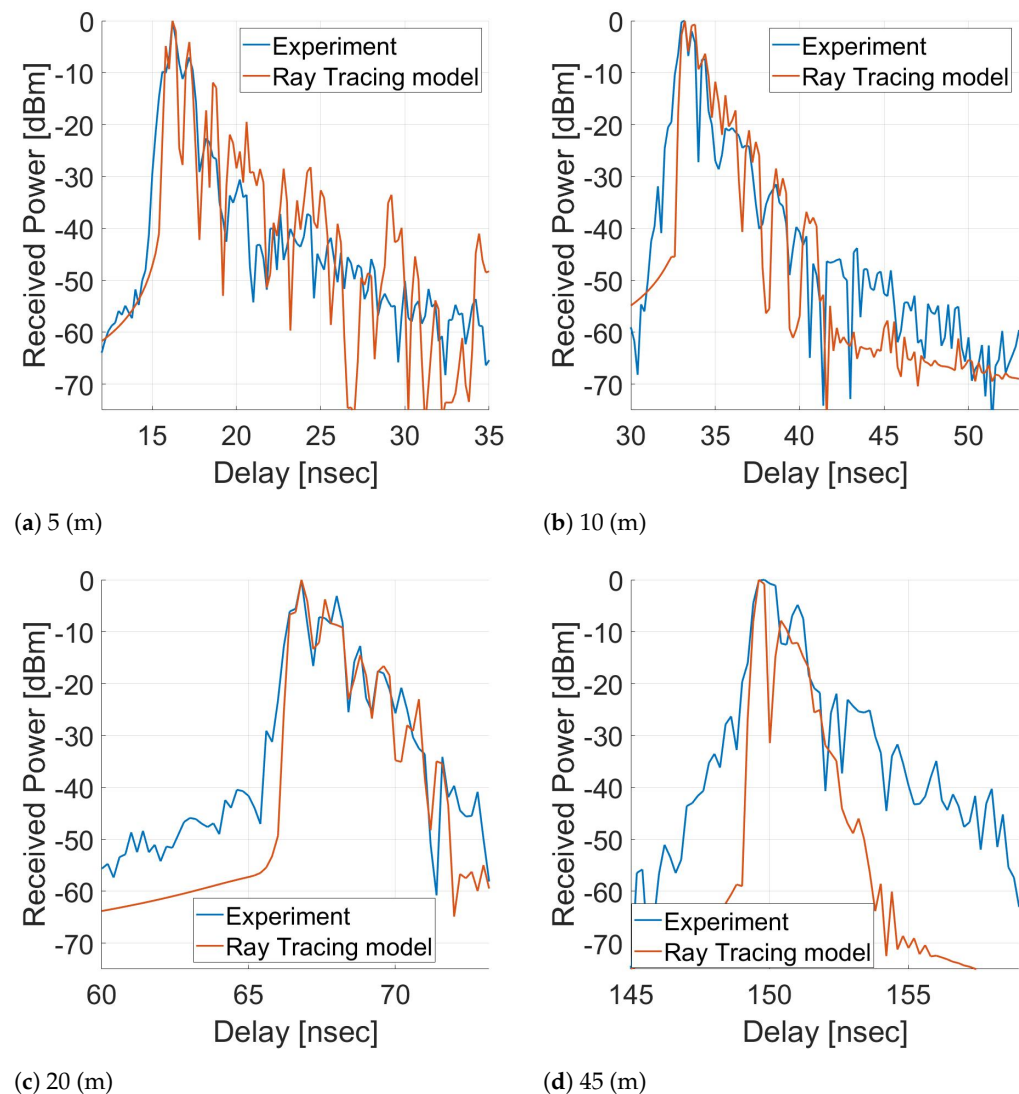


Figure 8. The time domain response of the transmission scattering parameter S_{21} for various distances.

This visualization of the experiment and simulation data can offer a clearer understanding of the multi-path components that reflect off the walls on their way to the receiver. The multi-path components can challenge the use of high data rates [28,29]. The PDP plot demonstrates the different rays received at the receiver.

For example, in the case of a 5 m gap between the transmitter and the receiver, the LOS ray reaches the receiver after a flight time of $t_{LOS} = 5/c \approx 17$ ns where c is the speed of light. This phenomenon can be observed in Figure 8a. The LOS ray arrives first with the strongest power at 17 ns, and subsequently the rest of the rays arrive with decreasing power.

Although there is an excellent fit between the experiment and the ray-tracing model throughout the entire pulse, as can be seen in Figure 8a, as the distance between the transmitter and receiver increases, the fit is greater in the main area of the pulse and there is

less fit at the beginning and end. This phenomenon is due to the fact that since the received power was obviously decreasing along the tunnel, the experiment setup was nearing the noise threshold. In addition, although the tunnel is almost completely flat, it still has a certain roughness. The effect of the roughness intensifies as you progress along the tunnel, and each ray may disperse several more times beyond what is calculated in the model. Despite all this, there is still a perfect match in the main and important part of the results, and the differences only occur with a difference of over 30 dB.

In order to obtain a broad observation of the tunnels' influence on the wide-band communication, a 3D plot of the PDP throughout the tunnel is shown in Figure 9.

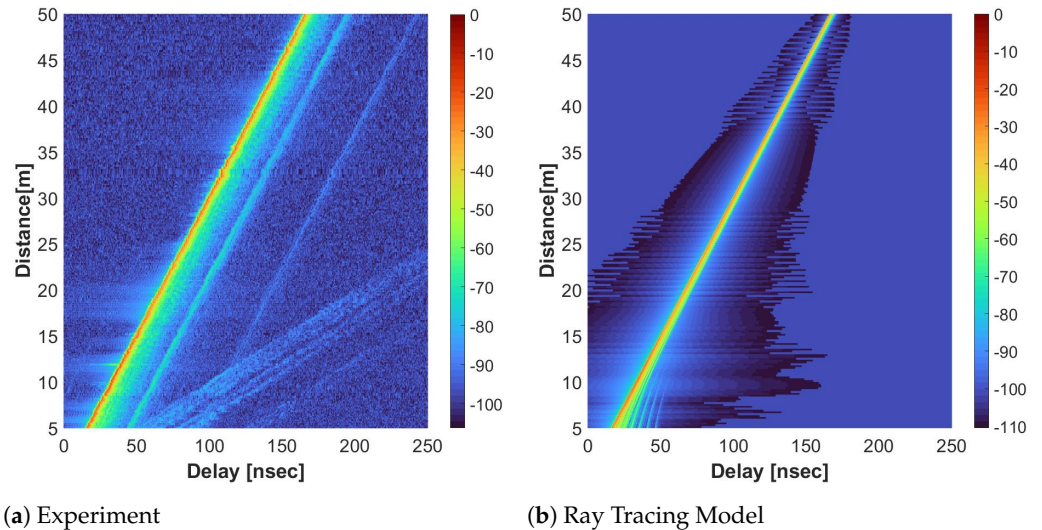


Figure 9. 3D plot of the PDP throughout the tunnel.

As can be observed in Figure 9, the LOS ray is absorbed at the receiver with a time suitable to the speed of light. This means that the LOS ray is received first at the receiver, followed by the rest of the rays which have been reflected multiple times off the walls of the tunnels. It can be recognized that the main phenomena remain commensurate along the tunnel, and with high similarity between the experiment and simulation.

As described in Section 2, the average delay and RMS delay spread were calculated with the data obtained from the experiment and simulation. A comparison between the experiment and simulation data is shown in Table 7.

The mean delay, $\bar{\tau}$, remains almost at the same value along the tunnel. The differences that can be noticed between the experiment and the model are within the resolution range of the measurement setup, as mentioned previously.

A parameter with a significant value in wide-band communication is the RMS delay spread, as defined in Equation (12). RMS delay spread can accurately convey the message of whether a communication link is possible in the current medium and distance [28]. The RMS delay spread is presented as a function of the distance between the Tx and Rx, as visible in Figure 10.

Table 7. Average and RMS delay spread for various distances.

| Distance (m) | Mean Delay Spread $\bar{\tau}$ (ns) | | RMS Delay Spread σ_{τ} (ns) | |
|--------------|-------------------------------------|------------|---------------------------------------|------------|
| | Experiment | Simulation | Experiment | Simulation |
| 5 | 3.4 | 3.2 | 0.78 | 0.85 |
| 10 | 2.4 | 2.65 | 0.62 | 0.63 |
| 20 | 2.6 | 2.85 | 0.66 | 0.67 |
| 45 | 2.3 | 2.4 | 0.41 | 0.44 |

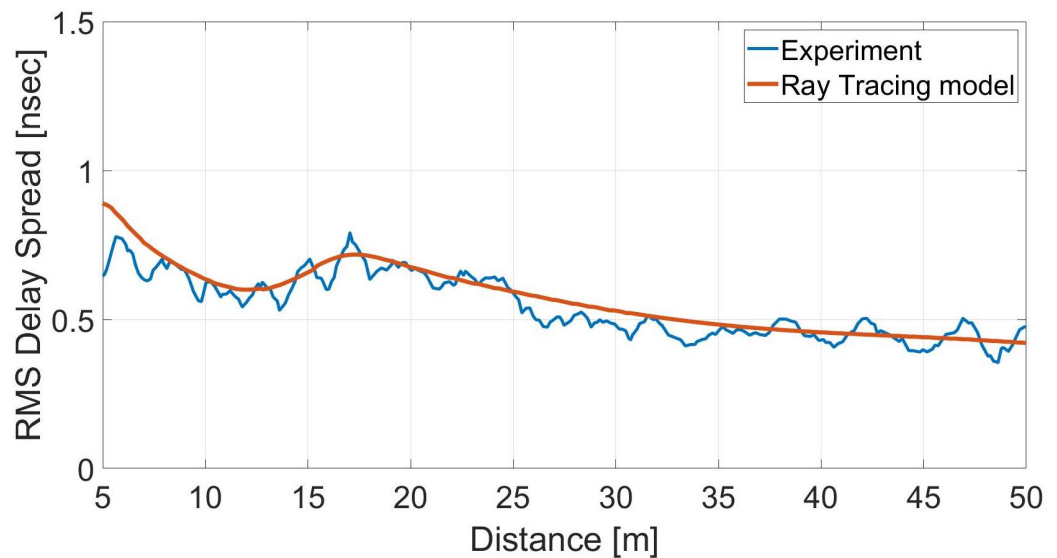


Figure 10. RMS delay spread comparison between the experiment and simulation.

The RMS delay spread, σ_τ , throughout the tunnel remains smaller than 1 ns. The value of 1 ns is significantly lower than other typical values, as shown in Table 1, but is similar to the values obtained in comparable studies [14]. Since the time resolution in the experiment is 0.2 ns and the value of the RMS delay spread is greater than that, the result obtained is accurate.

As noticeable, the RMS delay spread, σ_τ , is not a constant value along the tunnel. As mentioned, the antennas that were used are directional. When the range between the transmitter and receiver is small, a small number of rays reach the receiving antenna, but in high scatter, due to the large difference in the optical paths.

The farther away from the transmitter the receiver progresses, the smaller the difference in the optical paths becomes and then the scatter becomes smaller.

However, due to the directional characteristics of the antenna, at some point, additional rays that bounced off the walls begin to reach the receiving antenna, increasing the RMS delay spread.

After this stage, as the distance between the transmitter and the receiver increases, the RMS delay spread, σ_τ , dwindles down. The difference in the optical paths between the rays that do not experience strong decay becomes smaller, and the scattering from here on out becomes smaller. In other words, the rays that are reflected several times no longer reach the receiver with any significant power. The rays that remain powerful enough to get to the receiver are the rays that are reflected infrequently or not at all, and their travel time is similar to the time of the LOS ray.

A comparison between the average values along the whole tunnel of the experiment and the model is shown in Table 8.

Table 8. Summary Results.

| Parameter | Symbol | Experiment | Simulation |
|-------------------|---------------|------------|------------|
| Spread Delay (ns) | σ_τ | 0.55 | 0.54 |

6. Discussion and Conclusions

This study discusses an extensive measurement campaign that was carried out in a pedestrian tunnel, in which various parameters were measured, including the delay spread. The results of the measurements obtained were processed to show their enormous significance in characterizing the limitations of wireless communication in tunnels. The main feature of pedestrian tunnels is the fact that they are narrow and long in relation to

their width and height. This unique characteristic affects the arrival time of the LOS ray in comparison to the time of arrival of the rays reflecting off the walls.

Using our theory, as described in Section 2, an analysis was made of the received power and the delays in the arrival of the signal at the receiver as a result of the distance between the transmitter and the receiver. To validate the model, a wide-band experiment was performed using a VNA, which provided us with high-resolution measurements. With the use of optical means, the ability to receive the signal accurately was achieved. The results were presented, in Section 4, in the form of a comparison with the results of the theory, and as can be observed there is an excellent fit.

One of the main characteristics of the pedestrian tunnel is that the RMS delay spread, σ_τ , decreases along the tunnel. This can be explained by the fact that as the distance increases the rays returning from the walls have a lower power due to the attenuation created by the reflections from the wall. This is in contrast to the direct LOS ray, with the only effect on it being free space loss, which is lower. The sizes obtained, mean and RMS delay spread are of the same order of magnitude as the results obtained in previous studies that were performed in areas with similar topography. In contrast to the previous studies, this research is the most in-depth and comprehensive study of communication limitations in the pedestrian tunnel.

As was presented, there is a process of dispersion within the tunnel that is affected by Multi path, the effect of the dispersion on the communication channel may cause inter-symbol interference and should be considered in channel design.

Author Contributions: Conceptualization, Y.T., Y.P. and L.R.; methodology, Y.T. and Y.P.; software, Y.T., L.R. and G.A.P.; validation, Y.P.; formal analysis, Y.T.; investigation, Y.T., L.R. and Y.P.; resources, Y.T., L.R., N.E. and G.A.P.; data curation, Y.T. and N.E.; writing, original draft preparation, Y.T.; writing, review and editing, Y.T.; visualization, Y.T. and Y.P.; supervision, Y.P.; project administration, Y.P.; funding acquisition, Y.P. All authors have read and agreed to the published version of the manuscript.

Funding: This research received no external funding.

Acknowledgments: The first and third authors, Yehuda Taragin and Niv Elkayam would like to thank the Department of Advanced Studies of Ariel University for the scholarship and help. Also, this paper is part of Yehuda Taragin's PhD thesis and Niv Elkayam PhD thesis.

Conflicts of Interest: The authors declare no conflict of interest.

References

1. Turner, A. How Many Smartphones Are in the World? Available online: <https://www.bankmycell.com/blog/how-many-phones-are-in-the-world> (accessed on 5 April 2022).
2. Saad, W.; Bennis, M.; Chen, M. A Vision of 6G Wireless Systems: Applications, Trends, Technologies, and Open Research Problems. *IEEE Netw.* **2020**, *34*, 134–142. [[CrossRef](#)]
3. Kennedy, G.A.; Bedford, M.D. Underground wireless networking: A performance evaluation of communication standards for tunnelling and mining. *Tunn. Undergr. Space Technol.* **2014**, *43*, 157–170. [[CrossRef](#)]
4. Cox, D.; Leck, R. Distributions of multipath delay spread and average excess delay for 910-MHz urban mobile radio paths. *IEEE Trans. Antennas Propag.* **1975**, *23*, 206–213. [[CrossRef](#)]
5. Saleh, A.; Valenzuela, R. A Statistical Model for Indoor Multipath Propagation. *IEEE J. Sel. Areas Commun.* **1987**, *5*, 128–137. [[CrossRef](#)]
6. Chehri, A.; Fortier, P.; Tardif, P.M. CTHp1-8: Measurements and Modeling of Line-of-Sight UWB Channel in Underground Mines. In Proceedings of the IEEE Globecom 2006, San Francisco, CA, USA, 27 November–1 December 2006; pp. 1–5. [[CrossRef](#)]
7. Benzakour, A.; Affes, S.; Despins, C.; Tardif, P.M. RMS Delay Spread and Coherence Bandwidth Measurements in an Underground Mining Environment at 2.4 and 5.8 GHz. In Proceedings of the First International Workshop on Wireless Communication in Underground and Confined Areas, Val d'Or, QC, Canada, 6–7 June 2005.
8. Nobles, P.; Halsall, F. Delay spread measurements within a building at 2 GHz, 5 GHz and 17 GHz. In Proceedings of the IEE Colloquium on Propagation Aspects of Future Mobile Systems (Digest No: 1996/220), London, UK, 14 April–17 April 1996; pp. 8/1–8/6. [[CrossRef](#)]
9. Pérez, J.R.; Torres, R.P.; Rubio, L.; Basterrechea, J.; Domingo, M.; Peñarrocha, V.M.R.; Reig, J. Empirical Characterization of the Indoor Radio Channel for Array Antenna Systems in the 3 to 4 GHz Frequency Band. *IEEE Access* **2019**, *7*, 94725–94736. [[CrossRef](#)]

10. Rubio, L.; Reig, J.; Fernández, H.; Rodrigo-Peñarrocha, V. Experimental UWB Propagation Channel Path Loss and Time-Dispersion Characterization in a Laboratory Environment. *Int. J. Antennas Propag.* **2013**, *2013*, 350167. [CrossRef]
11. Wang, Y.; Lu, W.J.; Zhu, H.B. Propagation Characteristics of the LTE Indoor Radio Channel With Persons at 2.6 GHz. *IEEE Antennas Wirel. Propag. Lett.* **2013**, *12*, 991–994. [CrossRef]
12. Janssen, G.; Stigter, P.; Prasad, R. Wideband indoor channel measurements and BER analysis of frequency selective multipath channels at 2.4, 4.75, and 11.5 GHz. *IEEE Trans. Commun.* **1996**, *44*, 1272–1288. [CrossRef]
13. Huang, F.; Tian, L.; Zheng, Y.; Zhang, J. Propagation Characteristics of Indoor Radio Channel from 3.5 GHz to 28 GHz. In Proceedings of the 2016 IEEE 84th Vehicular Technology Conference (VTC-Fall), Montreal, QC, Canada, 18–21 September 2016; pp. 1–5. [CrossRef]
14. Garcia-Pardo, C.; Molina-Garcia-Pardo, J.M.; Lienard, M.; Degauque, P. Time Domain Analysis of Propagation Channels in Tunnels. In Proceedings of the 2011 7th International Conference on Wireless Communications, Networking and Mobile Computing (WiCOM 2011), Wuhan, China, 23–25 September 2011.
15. Da Silva, A.; Nakagawa, M. Performance investigation of OFDM communication systems in tunnels. In Proceedings of the Gateway to 21st Century Communications Village. VTC 1999-Fall. IEEE VTS 50th Vehicular Technology Conference (Cat. No.99CH36324), Amsterdam, The Netherlands, 19–22 September 1999; Volume 5, pp. 2908–2912. [CrossRef]
16. Chen, C.H.; Chiu, C.C.; Hung, S.C.; Lin, C.H. BER Performance of Wireless BPSK Communication System in Tunnels With and Without Traffic. *Wirel. Pers. Commun.* **2004**, *30*, 1–12. [CrossRef]
17. Debaenst, W.; Feys, A.; Cuiñas, I.; García Sánchez, M.; Verhaever, J. RMS Delay Spread vs. Coherence Bandwidth from 5G Indoor Radio Channel Measurements at 3.5 GHz Band. *Sensors* **2020**, *20*, 750. [CrossRef] [PubMed]
18. Varela, M.; Sanchez, M. RMS delay and coherence bandwidth measurements in indoor radio channels in the UHF band. *IEEE Trans. Veh. Technol.* **2001**, *50*, 515–525. [CrossRef]
19. Bashir, S. Effect of Antenna Position and Polarization on UWB Propagation Channel in Underground Mines and Tunnels. *IEEE Trans. Antennas Propag.* **2014**, *62*, 4771–4779. [CrossRef]
20. Zhang, Y.; Hwang, Y. Characterization of UHF radio propagation channels in tunnel environments for microcellular and personal communications. *IEEE Trans. Veh. Technol.* **1998**, *47*, 283–296. [CrossRef]
21. Molina-Garcia-Pardo, J.M.; Lienard, M.; Degauque, P.; Garcia-Pardo, C.; Juan-Llacer, L. MIMO Channel Capacity With Polarization Diversity in Arched Tunnels. *IEEE Antennas Wirel. Propag. Lett.* **2009**, *8*, 1186–1189. [CrossRef]
22. Zhou, C.; Plass, T.; Jacksha, R.; Waynert, J.A. RF Propagation in Mines and Tunnels: Extensive measurements for vertically, horizontally, and cross-polarized signals in mines and tunnels. *IEEE Antennas Propag. Mag.* **2015**, *57*, 88–102. [CrossRef]
23. Rapaport, L.; Pinhasi, G.A.; Pinhasi, Y. Millimeter Wave Propagation in Long Corridors and Tunnels—Theoretical Model and Experimental Verification. *Electronics* **2020**, *9*, 707. [CrossRef]
24. Rapaport, L.; Etinger, A.; Litvak, B.; Pinhasi, G.; Pinhasi, Y. Quasi Optical Multi-Ray Model For Wireless Communication Link in Millimeter Wavelengths. In Proceedings of the MATEC Web of Conferences, Cape Town, South Africa, 3–5 October 2018; EDP Sciences: Les Ulis, France, 2018; Volume 210, p. 03006.
25. Molisch, A.F. *Wireless Communications*, 2nd ed.; Wiley Publishing: Hoboken, NJ, USA, 2011.
26. Fotohabady, V.; Said, F. The effect of channel's delay spread on the efficiency of OFDM system. In Proceedings of the 2014 22nd Iranian Conference on Electrical Engineering (ICEE), Tehran, Iran, 20–22 May 2014; pp. 1848–1853. [CrossRef]
27. RFOptic. Programmable 6.0GHz RF over Fiber. Available online: <https://rfoptic.com/wp-content/uploads/2021/07/RFoF-6.0GHz-July2021.pdf> (accessed on 15 November 2021).
28. Chuang, J. The Effects of Time Delay Spread on Portable Radio Communications Channels with Digital Modulation. *IEEE J. Sel. Areas Commun.* **1987**, *5*, 879–889. [CrossRef]
29. Zahedi, Y.; Ngah, R.; Nunoo, S.; Mokayef, M.; Alavi, S.; Amiri, I. Experimental measurement and statistical analysis of the RMS delay spread in time-varying ultra-wideband communication channel. *Measurement* **2016**, *89*, 179–188. [CrossRef]